POLITECNICO DI TORINO
Repository ISTITUZIONALE

Aging of Historical Masonry Towers: The Garisenda Case Study

Original
Aging of Historical Masonry Towers: The Garisenda Case Study / Invernizzi, S., Lacidogna, G., Di Tommaso, A., Montanari, P.M.. - 753:(2025), pp. 534-548. (8th International Conference on Mechanics of Masonry Structures Strengthened with Composite Materials, MuRiCo8 2025 Bologna (Italy) June 25–27, 2025) [10.1007/978-3-032-05032-8_41].

Availability:
This version is available at: 11583/3005215 since: 2025-11-17T13:32:35Z

Publisher:
Springer

Published
DOI:10.1007/978-3-032-05032-8_41

Terms of use:

This article is made available under terms and conditions as specified in the corresponding bibliographic description in the repository

Publisher copyright
Springer postprint/Author's Accepted Manuscript (book chapters)

This is a post-peer-review, pre-copyedit version of a book chapter published in Mechanics of Masonry Structures Strengthened with Composite Materials. The final authenticated version is available online at: http://dx.doi.org/10.1007/978-3-032-05032-8_41

(Article begins on next page)

27 November 2026

Aging of historical masonry towers: the Garisenda case study

Stefano Invernizzi[1], Giuseppe Lacidogna[1], Angelo Di Tommaso[2], Pedro Marin Montanari[1]

[1] Department of Civil, Environmental, and Building Engineering (DISEG), Politecnico di Torino, Turin, Italy
[2] Accademia delle Scienze di Bologna, Bologna, Italy

Abstract The monitoring of ancient masonry towers highlights the daily and seasonal cyclic deformation due to the differential heating of the faces and core of the structure. For medieval towers, built around the XII Century, approximately 1,000 annual and 300,000 daily cycles must be considered. In terms of fatigue, the seasonal cyclic phenomenon is at the upper limit of the so-called low-cycle fatigue (LCF), while the phenomenon due to daily cycles ascribes to high-cycle fatigue (HCF). Some authors have conjectured that these phenomena may have been the cause of particularly sudden collapses in combination with time-dependent aspects such as creeps and diffusion phenomena [1, 2]. In this work we analyse the Garisenda Tower in Bologna (Italy). The evolution of the tower eccentricity is monitored by means of a pendulum, while the deformations of the selenite basement walls are measured by means of optical chords deformometers. In addition, the slow decay and microcracking progression in mortars and stone blocks is detected by monitoring Acoustic Emission (AE). The information acquired by the monitoring is combined with the measured temperatures to distinguish be-tween reversible and permanent deformations, the latter due to progressive damage accumulation [3–5]. The comparison is carried out with FEM numerical simulations of the tower evolution and experimental tests on Selenite stone specimens characterizing the block masonry of the tower basement. This analysis allows to improve the understanding of the phenomenon and helps the development of more reliable warning procedures for unstable damage progression and possible collapse.

Keywords Cultural Heritage, Masonry Tower, Non-destructive Techniques Monitoring, Finite Element Modelling, Structural Assessment

1 Introduction

The Garisenda Tower, situated in Bologna, Italy, is a paradigmatic example of medieval architecture that has been a distinctive feature of the city's skyline for several centuries. Constructed in the 12th century in conjunction with the Asinelli Tower, the edifice was commissioned by the influential Garisendi family, from whom it derives its nomenclature. However, the tower's structural integrity was compromised in 1351 due to problems in the foundation, resulting in a pronounced inclination. To mitigate potential safety risks, the tower's height was subsequently reduced by 13 meters. Currently, the tower stands at a height of 48 meters, exhibiting a notable lean of 3.22 meters Eastwards.

The tower has been monitored and assessed from a structural point of view for more than a century [6], while more recently researchers have conducted extensive studies to assess the tower's stability using non-invasive testing methods, including the use of piezoelectric sensors to detect internal acoustic emissions and fiber optic sensors to measure strain and temperature changes. The present research is particularly focused on the discrimination between reversible and permanent amounts of the tower deformations considering thermomechanical effects.

2 Materials and Methods

2.1 Pendulum

In February 2021, a 30-meter-long pendulum was installed inside the tower to measure the planar movement of its top in comparison with basement. A visual representation of the pendulum's position inside the tower is provided in Fig. 1.

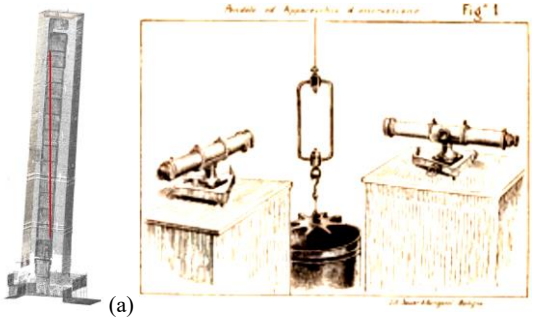

(a) (b)

Fig. 1 A representation of the pendulum inside the tower (a), courtesy of RTeknos, adapted from [3]. Scheme of the first pendulum installed in the Garisenda tower (b), adapted from [6].

The pendulum's automated acquisition can detect displacements of up to 100 mm in the south-east direction (X-axis) and up to 50 mm in the north-east direction (Y-axis). The pendulum has a margin of error of 0.075% of the maximum reading, translating to ±0.075 mm in the X direction and ±0.0375 mm in the Y direction. The internal temperature at the base of the tower is also recorded.

2.2 AE Monitoring

A specialized acoustic emission (AE) monitoring system was installed at the base of the Garisenda Tower to enable the real-time detection of structural anomalies. The system comprises two AE devices, designated AE001 and AE002, each configured with eight channels connected to eight piezoelectric sensors (model LT18-003-PRD00-R0) that part of a Lunitek AEmission network. The AE001 device was installed on May 31, 2019, while the AE002 device was subsequently installed on March 14, 2023, to enhance the monitoring capabilities. The sensors operate within a frequency range of 15-625 kHz, enabling the identification of damage-induced AE signals.

The system's data acquisition parameters are set to a sampling rate of 5 MS/s with a 16-bit resolution, allowing for the extraction of parametric data from the signals. To ensure a reliable and stable connection, the sensors are securely affixed to the tower's inner wall using a high-strength adhesive. A visual representation of the sensor installation and arrangement is provided in Fig. 2, which depicts the placement of the PZT sensors at the tower's base (left) and illustrates their schematic configuration (right).

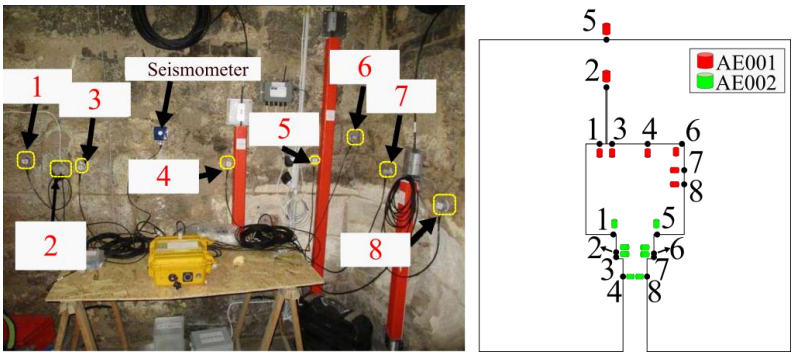

Fig. 2 The AE sensors *in-situ* (left) and a schematic of their disposition in the tower base (right). Adapted from [3].

2.3 FOS optical strand sensors monitoring

A monitoring system was implemented, using vertically installed Osmos optical strand sensors, to continuously monitor and record deformations at the base of the Garisenda Tower. Internal temperature measurements were also acquired. The data acquisition system operated at sampling frequency of 100 Hz, with a sensitivity of one microstrain (με), enabling the detection of subtle changes in the tower's deformation patterns. The collected data was transmitted to an advanced intelligent data acquisition unit (EDAS), where it underwent preprocessing, temporary storage, and subsequent transmission to a dedicated cloud-based server for long-term storage and analysis. The data was accessible and downloadable through a dedicated web-based platform, facilitating remote monitoring and data retrieval. Fig. 3 provides a visual representation of the optical string layout within the tower (a) and their schematic disposition in the tower base (b).

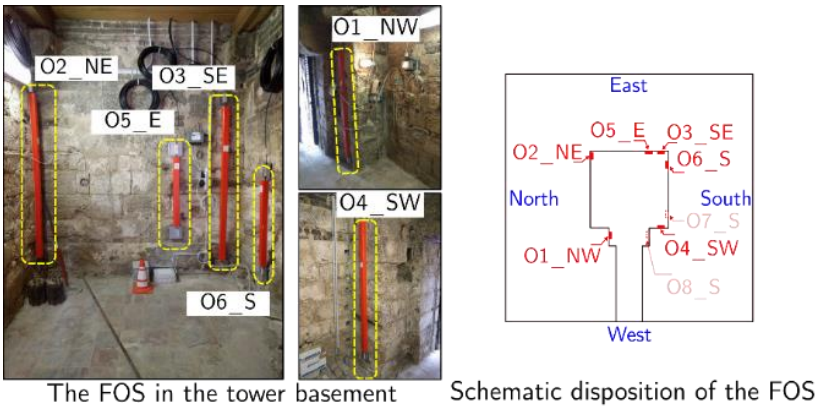

Fig. 3 The disposition of the optical strings inside the tower (left), the optical strings inside in the East wall of the tower base (right). Adapted from [3].

3 Results and discussion

3.1 Experimental

3.1.1 Relationship between AE and FOS strains

The FOS strains and the AE were analyzed together, see Fig. 4, to obtain insights into the evolution of the damage of the tower. The red vertical line refers to the date

of interdiction of the roads traffic near the Garisenda tower, which is nowadays still prescribed.

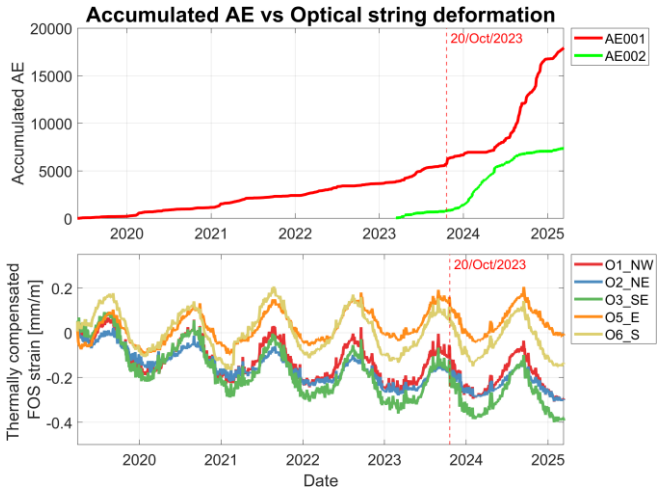

Fig. 4 The accumulated AE (top) and the FOS strains (bottom) from 30/Mar/2019 to 31/Mar/2025.

An examination of Fig. 4 reveals two distinct periods emerging in the relationship between Fiber Optic Sensor (FOS) strains and accumulated Acoustic Emissions (AE). The initial period, spanning from May 2019 to July 2023, exhibits a correlation between AE peaks and FOS minima, which coincide with the colder winter months (December-March). This suggests that thermal contraction of different layers may have contributed to damage in the tower's basement, inducing a change in compressive stress configuration. In contrast, a second period, starting around January 2024, is characterized by a decoupling of AE activity and colder temperatures, with significant increases in AE signals observed during hotter summer months (March-July). This shift in behavior may indicate a potentially critical situation, as AE activity appears to be becoming increasingly independent of environmental influences. A plausible explanation for this phenomenon is the onset of accelerated creep in the masonry, although further research is required to substantiate this hypothesis.

3.1.2 Mechanical characterization of the Selenite stone

The development of a precise finite element (FE) model for simulating the damage in the base of the tower requires two key material parameters: tensile fracture energy and compressive fracture energy. The fracture energy can be regarded as a quantitative measure of the material's resistance to tensile cracking, whereas the compressive fracture energy serves as an indicator of the material's resistance to progressive crushing.

To determine these material parameters, two comprehensive testing campaigns were conducted utilizing selenite specimens extracted from the tower's base. The first campaign employed three-point bending (TPB) tests to quantify the tensile fracture energy, while the second campaign utilized uniaxial compression tests to determine the compressive fracture energy. By conducting these experiments, the material properties were obtained, which then enabled the development of a robust and accurate FE model that can effectively simulate the damage evolution in the tower's base.

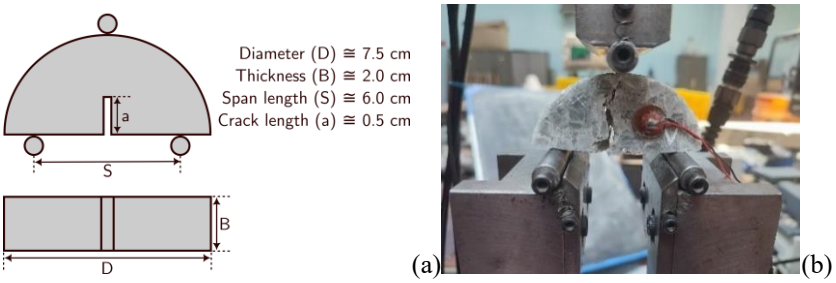

Fig. 5 A schematic of the TPB test specimen (a) and the specimen V after the TPB test (b).

The three-point bending tests were performed using three semicircular selenite samples (named specimens II, IV and V) gathered from the basement of the Garisenda tower. They had dimensions 75 mm (radius) × 20 mm (thickness) with a notch of 5 mm. A schematic of the sample and of the TPB testing procedure, as well as a picture of the V sample after the TPB test, can be seen in Fig. 5.

The calculation of the fracture energy was performed using the area under the load-displacement curve divided by the ligament area, with the displacement referring to the one of the piston of the hydraulic testing machine. The fracture energy G_F (N/m) was determined according to Eq. (1)

$$G_F = \frac{W_0}{A}. \tag{1}$$

Here, W_0 (J) is the area under the load-displacement curve, and A (m^2) is the ligament area. The fracture energy of the selenite was considered as the mean fracture energy calculated for the three samples. Fig. 6a presents the load-displacement curves from the TPB tests, while Fig. 6b summarizes the results.

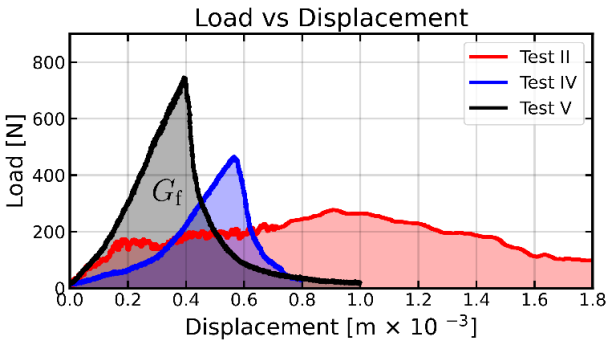

(a)

Sample	G_F (N/m)
II	358.30
IV	137.45
V	217.94
Mean	237.89

(b)

Fig. 6 The load-displacement curves from the TPB of the three specimens (a) and the fracture energy calculated from Eq. (1) (b).

The crushing tests were performed using six cylindrical selenite samples (named specimens 1-1, 1-2, 1-3, 2-1, 2-2, and 2-3) gathered from the basement of the Garisenda tower. The specimens 1-1, 1-2, and 1-3 had dimensions 100 mm (diameter) × 100 mm (height) while the specimens 2-1, 2-2, and 2-3 had dimensions 100 mm (diameter) × 200 mm (height).

The crushing energy was determined as the area under the softening branch of the stress-displacement curve. The displacement refers to the one of the piston of the hydraulic testing machine. The crushing energy G_c (N/m) was determined according to Eq. (2).

$$G_c = \sigma \cdot w_c \tag{2}$$

Here, σ (N/m^2) is the compressive stress, calculated as the load divided by the cross-section of the virgin specimens, and w_c (m) is the piston displacement. The crushing energy of the selenite was considered as the mean crushing energy calculated for the three samples. Fig. 7a presents the stress-displacement curves from the crushing tests, while Fig. 7b summarizes the results.

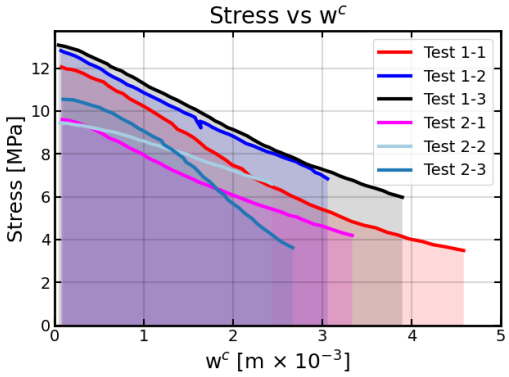

(a)

Specimen	G_c (N/m)
1-1	32.48×10^3
1-2	29.19×10^3
1-3	36.05×10^3
2-1	21.87×10^3
2-2	19.47×10^3
2-3	19.59×10^3
Mean	26.44×10^3

(b)

Fig. 7 Stress-displacement curves from the crushing of the six specimens (a), and values of the critical compression fracture energy (b).

It is interesting to note that the ratio of the mean crushing energy to the mean fracture energy is, Eq. (3)

$$\frac{G_c}{G_F} = \frac{26.44 \times 103}{237.89} = 111.14 \cong 100 \tag{3}$$

which is expected [7–9].

3.2 Numerical

3.2.1 Nonlinear FE model of the TPB tests

A nonlinear 2D plain-stress FE model of Experiment V was developed in DIANA (www.dianafea.com). This model enabled the calibration of the nonlinear material parameters for the Selenite stone, which were subsequently employed in the structural model of the Garisenda tower.

The FE model consisted of 2266 elements and 7038 nodes, and crack propagation was simulated using specialized interface elements equipped with fictitious elastic stiffness and a nonlinear cohesive law. The interface properties were defined as follows: normal and tangential fictitious stiffness of 1010 N/m3, tensile strength of 3.9 MPa, and bulk Young's modulus of 4.1 GPa.

The deformed shape of the model, as well as its load-displacement curve, is presented in Fig. 8, alongside the experimental results for comparison. The numerical model demonstrates a good reproduction of the experimental linear and softening

branches, with the peak load and peak load displacement being accurately approximated. Additionally, the accumulated number of AE signals is plotted in red, revealing that some AE events are detected experimentally prior to the peak load. In contrast, the numerical model predicts that the first crack propagation occurs almost immediately before the peak load, resulting in a more brittle crack pattern. This discrepancy can be attributed to the perfect localization of the cohesive crack in the numerical model, which leads to a more pronounced brittle behavior.

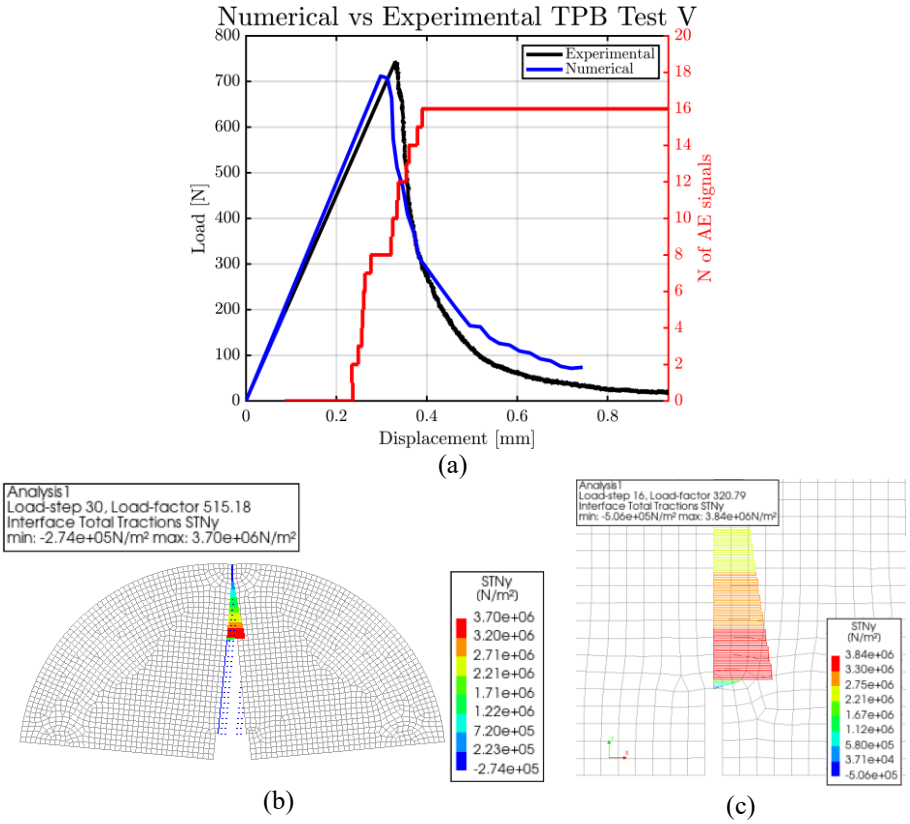

Fig. 8 Load-displacement curve measured at the node corresponding to the piston position in the testing machine (a), crack propagation and cohesive tractions on the interface elements (b), detail of the cohesive traction decrease in correspondence of first crack advancement (c).

3.2.2 Thermo-mechanical analysis of the tower

A finite element model of the whole tower and of the surrounding foundation soil was prepared to investigate the mechanical behaviour of the Garisenda accounting also for thermal deformations. The model was recently used to assess the effects of critical temperature scenarios [4].

The thermomechanical analysis was carried out according to a staggered solution scheme, where the heat transmission problem is solved first. Then, the mechanical problem is solved, which accounts for thermally induced deformation.

The boundary conditions for the initial problem were established by prescribing a known temperature field on both the external and internal surfaces of the tower. The external temperature field was determined through linear interpolation of four experimental measurements taken at the corners of the ashlar basement. In contrast, the internal temperature was assumed to be uniform, based on data from a single temperature sensor located within the tower. Furthermore, the temperature fields were height-invariant, simplifying the analysis and reducing the number of required thermomechanical material parameters. Under the assumption of steady-state heat transfer, which is reasonable for seasonal temperature variations, the thermal problem was analysed. However, to investigate the effects of daily temperature cycles, a transient heat transfer analysis would be necessary. In this study, the years 2023-2024 were considered, with temperature distributions evaluated at the beginning of each month at midnight to minimize the influence of weather patterns. Fig. 9 illustrates the temperature distribution at the start of June, as well as the corresponding stress increment in a cross-sectional plane of the tower basement.

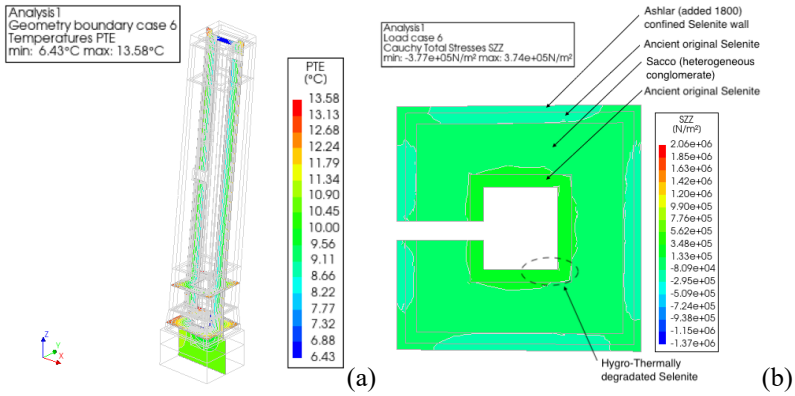

Fig. 9 Temperature distribution (a) and vertical stress increments due to thermal deformation at the basement section of the tower (b).

It can be noted that the stress increment in correspondence of the external Selenite layer is of the order of ± 0.5 MPa. If we consider a node in correspondence of the South-West internal corner of the tower basement for the period 11/2023-11/2024, as shown in Fig.10, it is possible to obtain the diagram of the vertical thermal stress increment versus time. In the same diagram, the local temperature is represented.

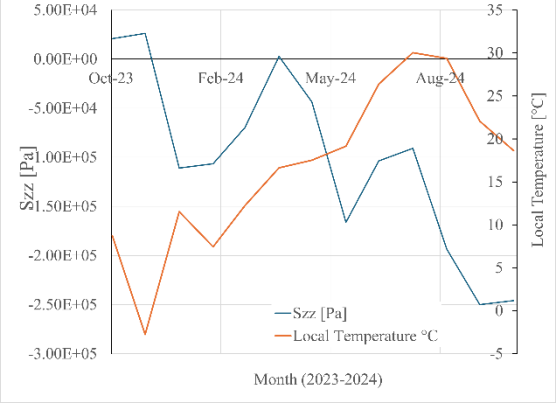

Fig. 10 Yearly stress variation due to temperature in correspondence of the S-E internal corner of the tower basement.

It is thus possible to estimate the yearly stress amplitude (about 0.5 MPa in this case) and to assess the effect of the thermal fatigue, the age of the tower being known. Of course, to provide a stability assessment, the fatigue characterization of the tower component materials would also be necessary.

In Fig. 11, the experimental and numerical strain in correspondence of the S-W internal corner of the tower is compared with the O7_S optical string. A good agreement is noticeable, with the sinusoidal trend seen from the *in-situ* data being well captured by the numerical model. At the end of the year, only a short amount of deformation (in the order of 0.1 mm/m) is not recovered.

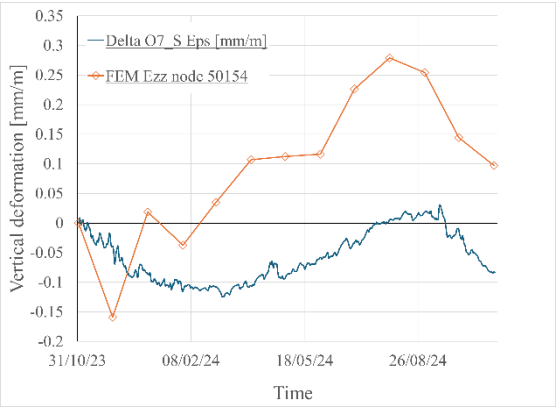

Fig 11. Experimental strain measurement at O3 FOS sensor, compared with the numerically calculated strains due to the temperature variation. For comparison, both values are calculated starting from the 1st of January 2023.

In addition, the evolution of the tower eccentricity acquired thanks to the pendulum can also be compared with the numerical results, in this case for the whole year of 2023. Again, for direct comparison reasons, all the measurements are taken as

increments starting from the first day of the 2023. Such results are depicted in the diagram shown in Fig. 12.

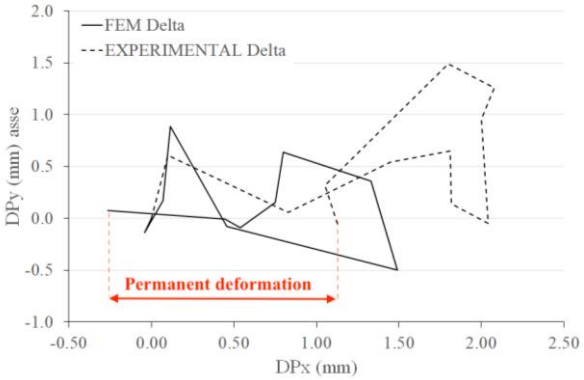

Fig. 12 Experimental and numerical evolution of the pendulum eccentricity. In red is the mismatch between calculated and measured eccentricity in the x direction.

In contrast to the previous case, a notable difference is evident regarding the eccentricity in the x-direction, which corresponds to an equivalent increase in the tower's lean towards the East. This finding is particularly noteworthy, as it makes it possible to distinguish reversible thermal-induced deformations and irreversible ones. Furthermore, this outcome is consistent with the results presented in Fig. 11, as the pendulum eccentricity is influenced not only by the tower's deformation but also by the rigid tilt of the tower induced by differential settlements of the foundation. In other words, a comparative analysis of the evidence presented in Figs. 11 and 12 suggests that the permanent deformation is likely attributable to the foundation tilt alone. Additionally, the magnitude of the irreversible deformation can also be inferred from the diagram in Fig. 13, although a definitive interpretation of the results remains challenging.

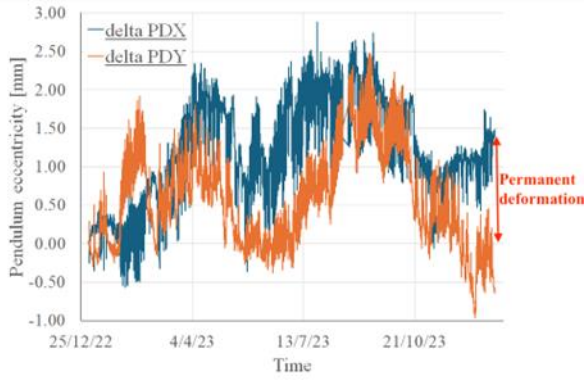

Fig. 13 Diagram of the eccentricity components yearly variation of the pendulum.

3.2.3 Damage assessment on the basement layers with nonlinear FEM and the AE technique

3.2.3.1 Nonlinear FEM

A preliminary structural nonlinear analysis was developed to investigate the cracking pattern induced by hypothetical further tilting of the foundation, with the objective of determining the additional inclination that could precipitate catastrophic failure. The constitutive behaviour of the materials at the base of the tower was modelled utilizing a Smeared Crack approach, which accounts for crack opening due to tension and plasticization due to compression.

The mechanical properties used in the numerical model are reported in Table 1.

Table 1: The mechanical properties used in the nonlinear FEM model

	E [Pa]	ν [-]	ρ [kg/m3]	σ_t [Pa]	G_f [N/m]	σ_c [Pa]	G_c [N/m]
Limous clay	1.5E8	0.3	1900	-	-	-	-
Brick masonry	3.5E9	0.2	1800	3.5E5	12	3.5E6	5600
Selenite masonry	4E9	0.2	2400	5E5	15.4	5E6	8000
Base filling	4E9	0.2	2200	6E5	17.5	6E6	9600
Elevation filling	2.5E9	0.2	1700	2.975E5	10.7	2.975E6	4760

These properties have been obtained experimentally [5] or from the literature [10–12]. The elastic properties have been validated by comparison of FEM modal analysis and experimental results [4].

The loading protocol consisted of a two-step process: (1) the application of the tower's self-weight, followed by (2) a settlement phase, wherein the tower was subjected to further rotation in the direction of its lean, simulating foundation subsidence and/or base wall settlement.

Fig. 14 shows the damage in the tower after approximately 2.5° of additional tilting.

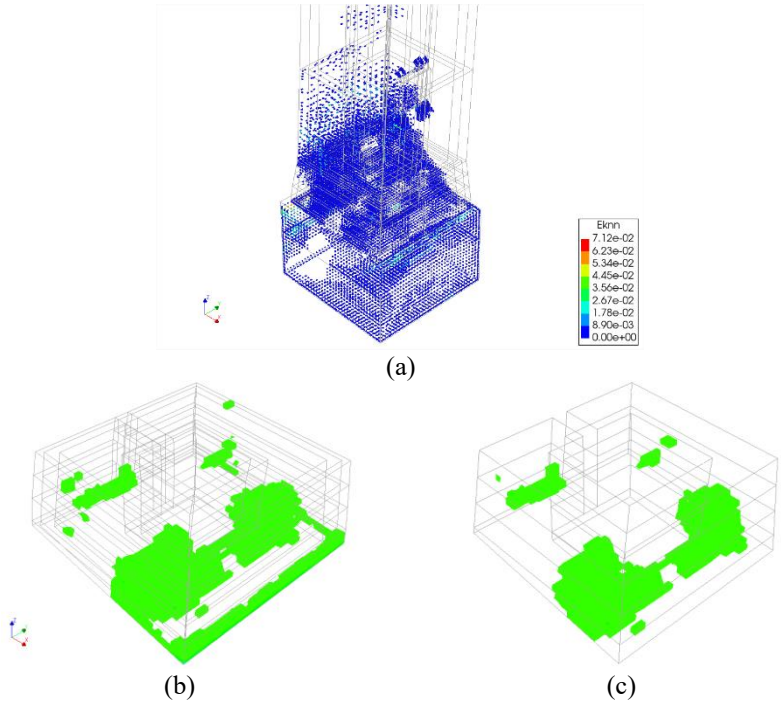

Fig. 14 The crack pattern developed in the lower part of the tower (a), the plasticized zones in all the layers of the tower base (b) and the plasticization of only the filling layer ("sacco").

Widespread cracking occurs, primarily concentrated in the westernmost region of the tower (the tensile region, opposite the leaning), while plasticization occurs mostly in the direction of leaning, where compression occurs.

Attention should be brought to the filling region ("sacco"). It is the layer where most of the plasticization occurs, as seen Fig. 13b-c, indicating it is the region most at structural risk.

It is important to note that in this preliminary model the interface between the material layers of the tower base is assumed as perfectly matched. This is an approximation of the actual configuration of the base of the Garisenda tower, as the interfaces are not perfectly coupled – for example, the outer selenite layer is damaged and badly connected to the outermost layer. The tower is also currently equipped with a containment structure consisting of steel cables that provide additional stiffness to the structure and help hold the layers together. This structure, or its effect, were not included in the preliminary model.

Furthermore, all materials are considered homogeneous, which is an idealization. Considering again the "sacco", it is known that, in the Middle Age, it was frequently built using all kinds of materials, even those inadequate to structural design. As such, it is a heterogeneous conglomerate by nature, and normally fragile and weak. In this sense, damage concentration in this layer can be expected. Even with the

previous hypotheses, the numerical model captures this behaviour. Further studies will focus on considering the materials in the tower base as heterogeneous materials with mechanical properties given by random fields.

3.2.3.2 AE Technique

Lastly, a study involving the AE technique was also performed, using AE data from the AE001 device, containing data from 24 January 2022 to 16 February 2025. A preliminary localization of AE events was also performed considering sensor pairs (CH1 + CH2, CH1 + CH3, …, CH5 + CH6). This localization, shown in Fig. 15a, allows to identify the distribution of AE signals by layer. Then, a frequency histogram of the AE signals perceived by each sensor individually was constructed, where the CH2 sensor (the one installed inside the "sacco") was put into highlight, as seen in Fig. 15b.

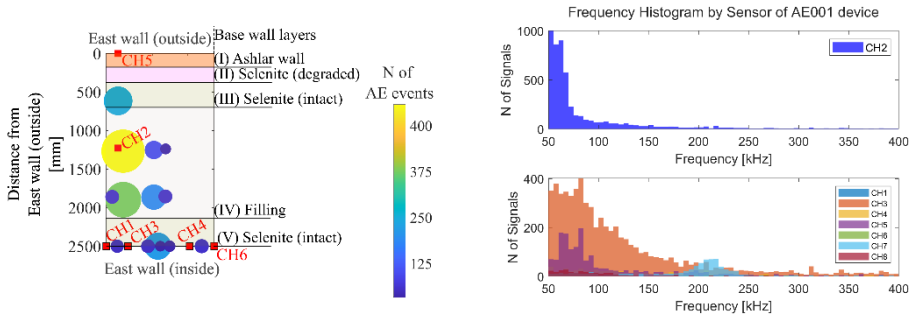

(a) (b)

Fig. 15 Preliminary localization of AE events through the thickness of the Garisenda base (a) and frequency histogram of AE signals of the AE001 device (b).

From Fig. 14a, the layer where most AE events occurs is the "sacco". Although a direct comparison cannot be made with the FE model, which considered an effect of tilting, the results are still relevant: both in the current situation (AE localization) and in the case of additional tilting (as seen by the FE model), damage seems more likely to occur in the "sacco".

The histogram in Fig. 15b depicts that, in the case of the sensor located inside the "sacco", CH2, most AE signals are contained in the low frequency range (50 – 100 kHz). Together with the localization with the spatial density of AE events, the frequency could be viewed as a kind of damage index to evaluate the structural health of the material layers. Other AE parameters (signal energy, amplitude, frequency, etc.) could also be candidates. In this sense, a more thorough damage index for the layers, based on AE parameters, will be discussed in further works.

4 Conclusions

In this work, a comprehensive approach integrating experimental and numerical methodologies was used to investigate the aging-induced damage at the base of the Garisenda tower in Bologna.

An analysis of the correlation between Fiber Optic Sensor (FOS) and Acoustic Emission (AE) data revealed a two-period scenario, with the initial period (until approximately July 2023) exhibiting a temperature-dependent increase in damage, whereas the subsequent period showed a temperature-independent increase in damage, potentially indicative of alternative dominant damage mechanisms, such as masonry aging and creep.

Furthermore, staggered steady-state thermomechanical finite element simulations were conducted to examine the effects of seasonal temperature variations on the Garisenda tower. Variations of stress that could be related to thermal fatigue were determined. A good agreement between FOS deformation and FE vertical strains was found. In relation to the pendulum movement, numerical and experimental results show a larger gap, although both allow to identify irreversible deformation trends in the tower and are thus indispensable for the structural health monitoring.

At last, nonlinear structural finite element analyses were built to investigate the damage of the tower in the case of additional leaning. Diffuse cracking occurs, and material plasticization is concentrated mostly on the “sacco” region. Comparisons of this behavior with *in-situ* AE data reveal the same trend and will allow in future works the investigation of damage indexes to assess structural health of the layers based on AE parameters.

The results demonstrated the utility of this approach in assessing the ongoing damage evolution and providing valuable insights into the tower's structural behavior.

Acknowledgments The authors wish to thank the Municipality of Bologna for providing part of the experimental data and for granting permission for publication.

References

[1] Anzani A, Garavaglia E, Binda L (2009) Long-term damage of historic masonry: A probabilistic model. Construction and Building Materials 23:713–724. https://doi.org/10.1016/j.conbuildmat.2008.02.010

[2] Ferretti D, Bažant ZP (2006) Stability of ancient masonry towers: Moisture diffusion, carbonation and size effect. Cement and Concrete Research 36:1379–1388. https://doi.org/10.1016/j.cemconres.2006.03.013

[3] Marin Montanari P, Lacidogna G, Invernizzi S, et al (2024) Experimental and Numerical Damage Assessment of the Garisenda Tower: Investigation by AE, Thermal, Seismic, and Permanent Strain Analyses. In: Rainieri C, Gentile C, Aenlle López M (eds) Proceedings of the 10th International Operational Modal Analysis Conference (IOMAC 2024). Springer Nature Switzerland, Cham, pp 3–14

[4] Invernizzi S, Lacidogna G, Olivetti GC, et al (2023) Garisenda Tower in Bologna (Italy): structural assessment and numerical simulation. IJMRI 1:1. https://doi.org/10.1504/IJMRI.2023.10053441

[5] Tommaso AD, Olivetti GC, Lacidogna G, et al (2024) Garisenda Tower in Bologna (Italy): health monitoring by different non-destructive testing techniques. IJMRI 9:54–66. https://doi.org/10.1504/IJMRI.2024.135248

[6] Cavani F (1901) Movimenti della sommità rispetto alla base nella torre Garisenda di bologna. Memorie della Regia Accademia delle Scienze dell'Istituto di Bologna – classe di scienze fisiche serie VI:317–330

[7] Carpinteri A, Corrado M, Paggi M, Mancini G Cohesive versus overlapping crack model for a size effect analysis of RC elements in bending

[8] Akiyama M, Hong K-N, Suzuki M, et al (2005) Concentric loading test of rc columns with normal- and high-strength materials and stress-strain model for confined concrete considering compressive fracture energy. Doboku Gakkai Ronbunshu 2005:788_81-788_98. https://doi.org/10.2208/jscej.2005.788_81

[9] Yang B, He M, Deng B, Zhang Z (2022) Correlation between the tensile to compressive strength ratio and mechanical parameters of rock based on a nonlinear M-C criterion. Arab J Geosci 15:928. https://doi.org/10.1007/s12517-022-10195-2

[10] Giordano F (2000) La torre Garisenda. Costa Editrice, Bologna

[11] Piccolo A (2017) Analisi strutturale delle così dette Due Torri di Bologna. Bachelor Thesis, Università di Bologna

[12] Comité euro-international du béton (1993) CEB-FIP model code 1990: design code. T. Telford, London